SO$_2$ sensing performance of chemically sprayed WO$_3$- V$_2$O$_5$ nanocomposites thin films

J. M. Patil*[1], S. B. Patil[2], R. H. Bari[2], and A. N. Sonar[1]

**[1]*Department of Chemistry, Shri. V. S. Naik, A.C.S. College, Raver, 425508, Maharashtra, India.
[2]Nanomaterials Research Laboratory, Department of Physics, G. D. M. Arts, K. R. N. Com. And M. D. Science College, Jamner, 424 206, Maharashtra, India.**

Abstract : WO$_3$, V$_2$O$_5$, and WO$_3$-V$_2$O$_5$ nanocomposites thin films were prepared by spray pyrolysis method onto the heated glass substrate at 350 ^{o}C. The films were fired at 500 ^{o}C. As prepared thin films were studied using XRD, FE-SEM and EDAX to know crystal structure, surface morphology and elemental composition. The gas sensing performance of pure WO$_3$, V$_2$O$_5$, and different composition of WO$_3$-V$_2$O$_5$ was studied on exposure of different conventional gases for 500 ppm. The film sprayed for composition of WO$_3$-V$_2$O$_5$ (Sample =S4) was observed to be most sensitive (S = 1130) to SO$_2$ at 350 ^{o}C. The sensor shows quick response (4 s) and fast recovery (8 s) time. The results are discussed and interpreted.

Keywords: Spray Pyrolysis, WO$_3$-V$_2$O$_5$ nanocomposites, SO$_2$ gas sensing, quick response, fast recovery.

1. Introduction

In the 21st century, human living standards have grown remarkably due to industrial revolution. On the other hand industrialization also affects the human health and environment due to emission of pollutant gases. Flammable gases need to be monitored to protect against unwanted incident of explosion and fire [1]. It has been known for a long time that electrical resistance of a semiconductor is very sensitive to the presence of impurities in its volume or at surface. Thus metal oxide semiconductors are used extensively as a sensing element of different gases and vapors. A depletion region always formed at the surface of metal oxide semiconductor due to adsorption of air oxygen molecules. Then the reaction with the target gas molecule causes reduction of depletion region which results change in conductivity of metal oxide semiconductor. The conductivity may increase or decrease depending on type of semiconductor and type of target gas [2].

Tungsten oxide (WO$_3$) is a transition metal oxide semiconductor with a widely band gap, in the range of Eg=2.5-2.8eV at room temperature. Interest was recently put on WO$_3$ thin films and nanoparticles [3]. WO$_3$ is n-type semiconductor that encloses interesting physical and chemical properties, that is why it is useful for a wide spectrum of technologies applications. For instance, tungsten oxide is an important material for electrochromic [4] and photoelectrochemical devices [5], catalyst [6] and gas sensors [7, 8].

Vanadium pentoxide is generally a non-stoichiometric material, which is known for its catalytic properties in oxidation reactions. Moreover, their use as components of gas sensors has been proposed [9]. The electrical transport mechanism in V$_2$O$_5$ fibres have been studied in detail [10]. V$_2$O$_5$ is an *n*-type semiconductor with an electronic conductivity in the order of 0.5 Scm^{-1} at room temperature [11].

The metal oxide-sensing layer (WO_3 or V_2O_5) has been fabricated in different physical forms such as thin film, thick films, and bulk pellets. However, the thin film form is expected to be most effective, because sensing is basically a surface phenomenon of film [12-13]. Thus, a very few work has been reported for the combination of WO_3/V_2O_5 oxide composite [14].

In present work efforts was done in the area of SO_2 detection using metal oxide thin films [15]. However, not much attention has been given to the fabrication of nanocomposites structure for detection of SO_2 gas. There has been intensive research on improving the gas sensitivity and selectivity by controlling the particle size [16], nanostructures [17, 18], sensing temperature [19], surface and structure [20].

Spray pyrolysis has proved to be simple, reproducible and inexpensive, as well as suitable for large area applications. Besides the simple experimental arrangement, high growth rate and mass production capability for large area coatings make them useful for industrial as well as solar cell applications. In addition, spray pyrolysis opens up the possibility to control the film morphology and particle size in the nanometer range [21].

We have tried to improve the fast detection and high response of SO_2 gas response by making composites of WO_3-V_2O_5 and found that WO_3 is a unique excellent promoter of the V_2O_5 gas sensor for the sensitive and selective detection of SO_2. This paper deals with the preparation of pure and composite thin films of WO_3, V_2O_5, and WO_3-V_2O_5. These films were studied using different analytical techniques. These WO_3, V_2O_5, and WO_3-V_2O_5 nanocomposites thin films were tested for sensing different gases and was observed to be most sensitive to SO_2 at 350 ^{0}C.

2. Experimental details

2.1 Preparation of pure WO_3, V_2O_5, and WO_3-V_2O_5 nanocomposites thin films

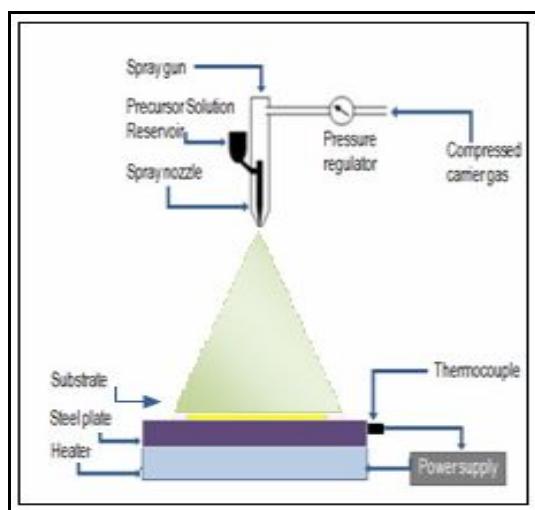**Figure 1: Schematic diagram of spray pyrolysis system for the preparation of WO_3, V_2O_5, and WO_3-V_2O_5 nanocomposites thin films**

Fig. 1 shows spray pyrolysis technique for preparation of pure WO_3, V_2O_5, and WO_3-V_2O_5 nanocomposites thin films. Set-up consists of spraying chamber, spray nozzle (gun), compressor for carrier gas, heating system, and temperature indicator.

2.2 Preparation of nanostructured WO_3 thin films

Nanostructured WO_3 thin films were prepared using the above set up. (0.05M) Tungsten hexachloride (WCl_6, Purified Merck) and N-N formamide (Solvent) was chosen as the starting solution for the preparation of the films. WCl_6 and N-N dimethyl formamide amine in 1:1 proportion were chosen for preparation of the thin films.

2.3 Preparation of nanostructured V_2O_5 thin films

V_2O_5 thin films were prepared by using Vanadium (III) chloride (VCl_3), Purified Aldrich) in de-ionized water as a precursor. A concentration of precursor solution (0.05M) was sprayed through a specially designed glass nozzle of 0.5 mm inner diameter onto the ultrasonically cleaned glass substrates.

2.4 Preparation of WO_3-V_2O_5 nanocomposites thin films

The starting material used for the preparation of WO_3-V_2O_5 nanocomposites thin films were tungsten hexachloride (WCl_6, Purified Merck) and vanadium (III) chloride (VCl_3), Purified Aldrich). Tungsten hexachloride and vanadium (III) chloride were mixed at various volume ratio such as 30:70, 50:50 and 70:30 as indicated in Table 1.

Table 1: Amounts of spraying solutions and reactant

Sample No.	WCl_6 (cm^3)	VCl_3 (cm^3)	Reactants
S1	-	100	WO_3
S2	100	-	V_2O_5
S3	30	70	WO_3:V_2O_5
S4	50	50	WO_3:V_2O_5
S5	70	30	WO_3:V_2O_5

The optimized deposition parameters like substrate temperature (350 ^{o}C), spray time (10 mn.), rate of spraying solution (8 ml/min.), nozzle to substrate distance (30 cm), quantity of the solution sprayed (30 ml), pressure of carrier gas, and to and fro movement of the nozzle were kept constant. The temperature of the substrate is maintained at a constant value by using a temperature controlled hot plate. The film formation depends upon the droplet landing, reaction and solvent evaporation, which relates to the droplet size. When the droplet approaches the substrate just before the solvent is completely removed, that is the ideal condition for the preparation of the pure WO_3, V_2O_5, and WO_3-V_2O_5 nanocomposites thin film.

2.5. Post preparative treatment

The as prepared WO_3, V_2O_5, and WO_3-V_2O_5 nanocomposites thin films samples (S1, S2, S3, S4 and S5) were annealed at 500 ^{o}C for 1 h.

2.6. Sensing system to test the gases

Fig. 2 shows block diagram of gas sensing system. The gas sensing studies were carried out using a static gas chamber to sense SO_2 gas in air ambient. The WO_3, V_2O_5, and WO_3-V_2O_5 nanocomposites thin films were used as the sensing elements. The sensing element was kept directly on a heater in the gas chamber and the temperature of the heater is controlled by controlling the current passing through the heater. The Cr-Al (chromel-alumel) thermocouple was used in contact with the sensor to sense the operating temperature of the sensor. The output of the thermocouple was connected to a digital temperature indicator.
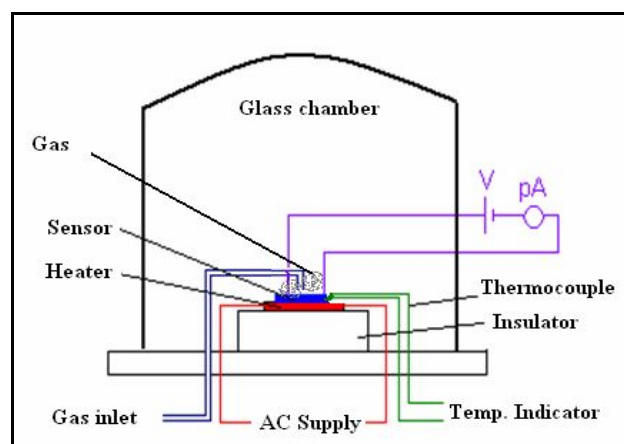

Figure 2: Block diagram of gas sensing system

The known volume of the SO_2 gas was introduced in to the gas chamber pre-filled with air and it was maintained at atmospheric pressure. A constant voltage (5V) was applied to the sensor and the current was measured by a digital picoammeter.

3. Characterizations of thin films

3.1. X-ray diffraction

The pure WO_3, V_2O_5, and WO_3-V_2O_5 nanocomposites thin films were characterized by X-ray diffraction (Miniflex Model, Rigaku, Japan)) using CuKα radiation with a wavelength, $\lambda = 1\cdot542$ Å. The average crystallite size of pure WO_3, V_2O_5, and WO_3-V_2O_5 nanocomposites thin film samples were calculated by using the Scherrer formula

$D = 0\cdot9\lambda/\beta\cos\theta$ ------------------------- (1)
Where, D = Average crystallite size
λ = X-ray wavelength (1·542 Å)
β = FWHM of the peak
θ = Diffraction peak position.

3.2. Surface Morphology

The surface morphology and elemental composition of the thin films were analyzed using Field emission scanning electron microscope (FE-SEM, JEOL. JED 6300) coupled with energy dispersive spectrophotometer (EDAX).

3.3 Gas sensing performance of thin films

3.3.1. Gas response

Gas response (S) of the sensor is defined as the ratio of change in conductance to the conductance of the sensor on exposure of target (at same operating conditions).

S =Ig-Ia/Ia   ---------------------------- (2)
Where, Ia = the conductance of the sensor in air
Ig = the conductance on exposure of a target gas.

3.3.2. Selectivity

The response of the sensor to a specific gas in the mixture of gases is the selectivity.

3.3.3. Response time

The time taken by the sensor to attain the 80% of maximum change in resistance on exposure to the gas is response time.

3.3.4. Recovery time

The time taken by the sensor to roll back to 80 % of its original resistance is the recovery time.

4. Results and discussion

4.1. Structural analysis using X-ray diffractogram

Fig. 3 shows the X-ray diffractogram of thin film samples S1, S2, S3, S4 and S5. The structural properties of the films were investigated using XRD. The *2θ* values were varied from 10 to 80°. The XRD patterns of WO_3 (for sample =S1) indicate hexagonal structure and V_2O_5 (for sample =S2) shows monoclinic structure. Sample S3- S5 indicates mixed phases of WO_3 (*) and V_2O_5 ($^+$).No other impurities was observed in XRD. XRD pattern revealed

that (for sample S3-S5) the formation of WO_3-V_2O_5 nanocomposites thin films. The WO_3 and V_2O_5 diffraction peaks are match with standard ASTM data WO_3 and V_2O_5 [22-23]. The observed peak predominates indicating a preferential growth. This means that the grains have *c*-axis perpendicular to the substrate surface. The calculated average crystallite sizes were presented in Table 3.
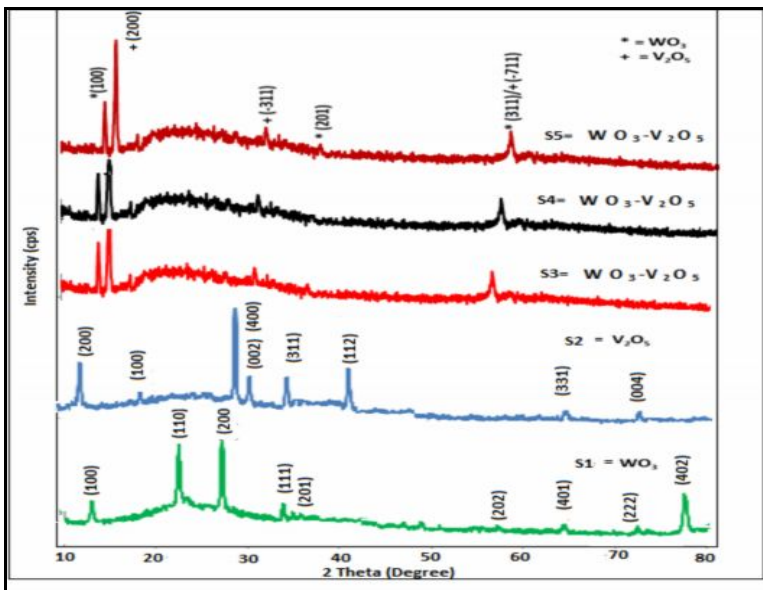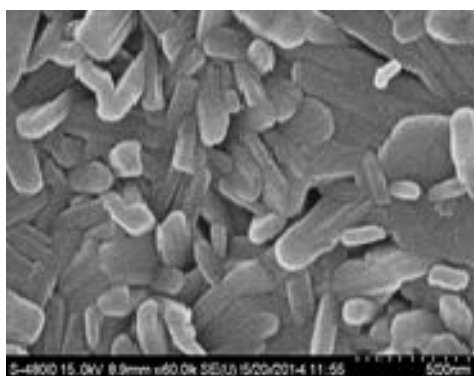

Figure 3: X-ray diffractogram of WO_3, V_2O_5, and WO_3-V_2O_5 nanocomposites thin films samples: (a) S1, (b) S2, (c) S3, (d) S4 and (e) S5
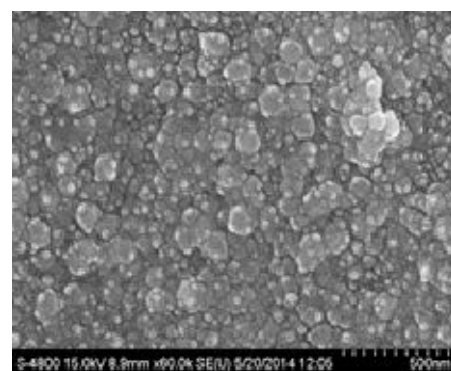
4.2. Surface Morphology

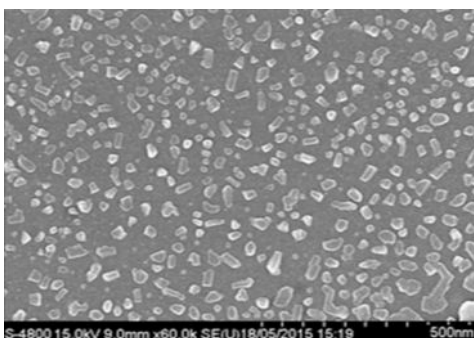### 4.2.1. Field emission scanning electron microscope

FE-SEM images of pure WO_3, V_2O_5, and WO_3-V_2O_5 nanocomposites were represented in Fig.4.

(a)

(b)

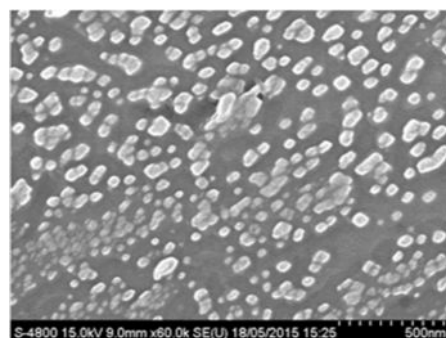
(c)
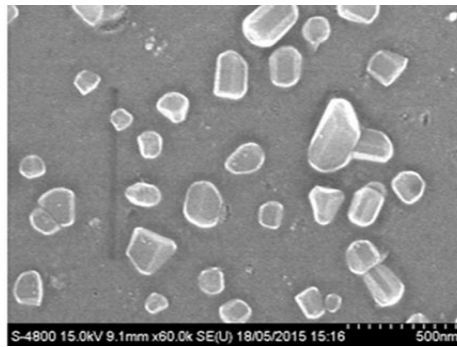

(d)

(e)

Figure 4: FE-SEM images pure WO$_3$, V$_2$O$_5$, and WO$_3$-V$_2$O$_5$ nanocomposites thin films: (a) S1, (b) S2, (c) S3 (d) S4 and (e) S5

Fig. 4 (a) shows the angular formation of the grain for WO$_3$ and for V$_2$O$_5$ grains were observed to be spherical in shape with different size. By increasing WO$_3$ % in V$_2$O$_5$ (Fig.4(c) (d) and (e)) thin films, the shape of the grains change into the mixed cubical and monoclinic phases. Grain size observed to be in the range of 21 - 44 nm.

4.3. Elemental composition using (EDAX)

The quantative element compositions of the thin film samples were analyzed using an energy dispersive spectrometer. Stoichiometrically expected at % of W and O is: 25 and 75 for WO$_3$. For V$_2$O$_5$ stoichiometrical expected at % is V:28.57, O: 71.43, and for WO$_3$-V$_2$O$_5$ at % of W ,V and O is : 9.09, 18.18 and 72.72, Observed at % for WO$_3$, V$_2$O$_5$, and WO$_3$-V$_2$O$_5$ nanocomposites thin films were given in Table 2.

Table 2: Quantative elemental analysis as prepared pure WO$_3$, V$_2$O$_5$, and WO$_3$-V$_2$O$_5$ nanocomposites thin film

Element	Observed									
	S1		**S2**		**S3**		**S4**		**S5**	
	wt %	at %	wt %	at %	wt %	at %	wt %	at %	wt %	at %
W	45.13	24.11	-	-	10.24	01.49	45.25	10.87	51.37	09.01
V	-	-	45.38	21.76	44.91	23.57	32.73	28.37	05.07	25.21
O	54.87	75.89	54.62	78.24	44.85	74.94	22.02	60.71	43.56	65.78
Total	100	100	100	100	100	100	100	100	100	100

It is clear from table 2, that as prepared pure WO$_3$, V$_2$O$_5$, and WO$_3$-V$_2$O$_5$ nanocomposites thin films were observed to be nonstoichiometric in nature. Sample S4 was observed to be more oxygen deficiency as compared to other samples, and it is favorable for gas sensor application.

4.4. Determination of film thickness

The film thickness was measured by a well-known weight difference method [24] in which weight of the sample, area and densities were considered. The thickness, sample weight and sample area are related as:

$t = M/A. \rho$ ----------------- (3)
Where, M is the weight of the sample in *gm,*
A the area of the sample in *cm^2*
and ρ the materials density in *gm cm^{-3}*.

The values of the film thickness with crystalline size are given in Table 3.

Table 3: Measurement of film thickness with crystalline and grain size

Sample No.	Thickness (nm)	Crystallite size calculated from XRD (nm)	Grain size observed from FE-SEM (nm)
S1	113	19	21
S2	124	24	37
S3	140	27	39
S4	156	29	41
S5	163	33	44

The thickness of the film was varied from 113 to 163 nm. It was found that the thickness of the film increases with increase of at % W in V_2O_5. It is also clear from table 3, that crystallite and grain size goes on increasing with increase in film thickness and mass % of W in V_2O_5.

4.5. Electrical properties

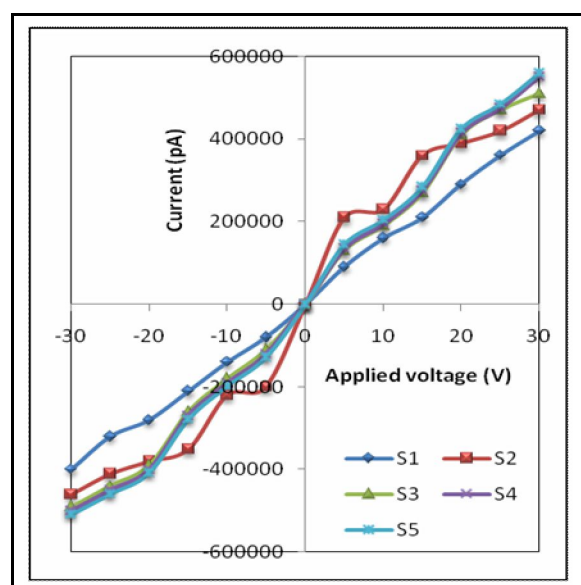### 4.5.1. I–V characteristics

Figure 5: I–V characteristics of nanocomposites thin film sensors: samples S1, S2, S3, S4 and S5.

Fig. 5 shows the I–V characteristics of samples S1, S2, S3, S4 and S5 observed to be nearly symmetrical in nature indicating ohmic nature of contacts. The non-linear I–V characteristics may be due to semiconducting nature of the films [25].

4.5.2. Electrical conductivity

Fig. 6 shows the variation of log (σ) with operating temperature. The conductivity of each sample is observed to be increasing with an increase in temperature. The increase in conductivity with increase in temperature could be attributed to negative temperature coefficient of resistance and semiconducting nature of the films.
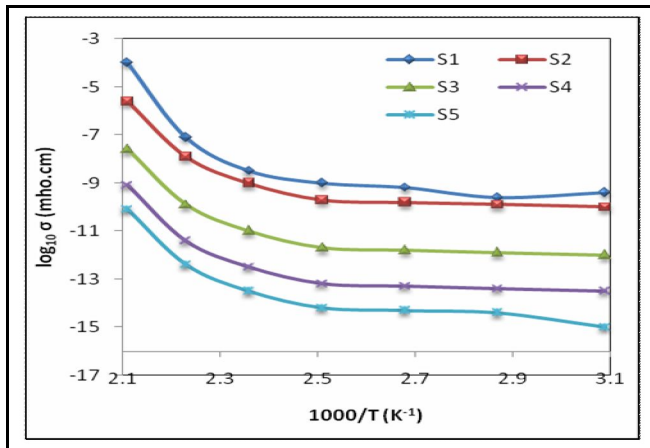
Figure 6: Variation of log (σ) with operating temperature (∘C).

It clearly indicates that the WO_3, V_2O_5, and WO_3-V_2O_5 nanocomposites thin films are semiconducting in nature [25].

5. Gas sensing performance of the sensors

5.1. Gas response

Fig. 7 represents the response characteristics of the WO_3, V_2O_5, and WO_3-V_2O_5 nanocomposite thin films as a function of operating temperature. Among all the films, the sample (S4) film shows the maximum response (1130) at 350 ^0C to 500 ppm of SO_2. At a low operating temperature of 200 ^0C, the response of the film to SO_2 is restricted by the speed of the chemical reaction. In fact, during adsorption of atmospheric oxygen on the film surface, a potential barrier to charge transport is developed. As a result, at low temperatures the SO_2 molecules do not have enough thermal energy to react with the surface adsorbed oxygen species.
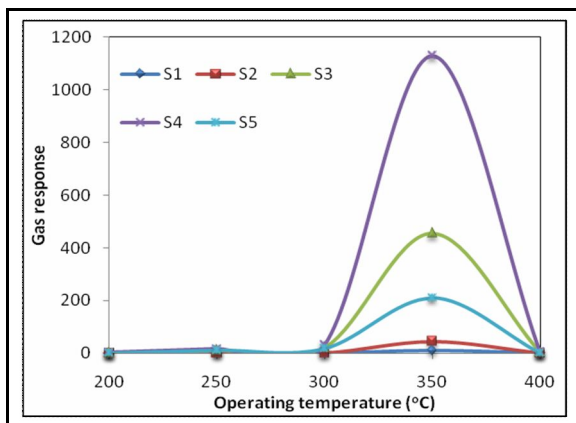

Figure 7: Gas response of nanocomposites thin films with operating temperature: samples S1, S2, S3, S4 and S5.

When the film is heated beyond 200 ^0C, the speed of chemical reaction enhances because of the availability of the sufficient thermal energy to overcome the potential barrier. All the films exhibit the maximum response to SO_2 at an operating temperature of 350 ^0C. This is attributed to the availability of the sufficient adsorbed ionic species of oxygen on the film surface which reacted most effectively with SO_2 at this particular temperature. At temperatures higher than 350 ^0C, the adsorbed oxygen species available at the sensing sites on the film surface are not enough to react with the SO_2. This results in a small change in resistance at higher temperatures. Therefore the response of the films begins to decrease at temperatures higher than 350 ^0C. In general, there exists an optimum operating temperature of a sensor to achieve the maximum response to a gas of interest, the temperature being dependent upon the kind of gases, i.e., the mechanism of dissociation and further chemisorptions of a gas on the particular sensor surface [26].

5.2. Selectivity

Fig 8 shows the histogram for comparison of the gas response to various gases for S1, S2, S3, S4 and S5 samples at the optimum operating temperature 350 °C. The table attached to histogram shows the response values, it is clear that the S4 film is highly selective to SO_2 (500 ppm) against all other tested gases: LPG, CO_2, H_2, NH_3, C_2H_5OH, CH_3OH, acetone, Cl_2 and H_2S.

Selectivity of gas
Con. of gas= 500 ppm
Op. temp.= 350 ^{0}C

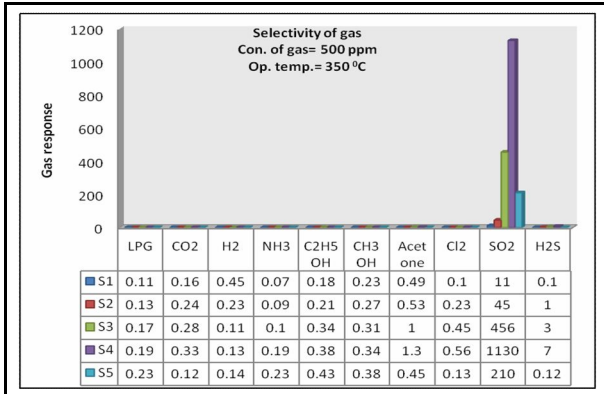|	LPG	CO2	H2	NH3	C2H5 OH	CH3 OH	Acet one	Cl2	SO2	H2S
S1	0.11	0.16	0.45	0.07	0.18	0.23	0.49	0.1	11	0.1
S2	0.13	0.24	0.23	0.09	0.21	0.27	0.53	0.23	45	1
S3	0.17	0.28	0.11	0.1	0.34	0.31	1	0.45	456	3
S4	0.19	0.33	0.13	0.19	0.38	0.34	1.3	0.56	1130	7
S5	0.23	0.12	0.14	0.23	0.43	0.38	0.45	0.13	210	0.12

Figure 8: Selectivity of nanocomposite thin films for different gases: samples S1, S2, S3, S4 and S5.

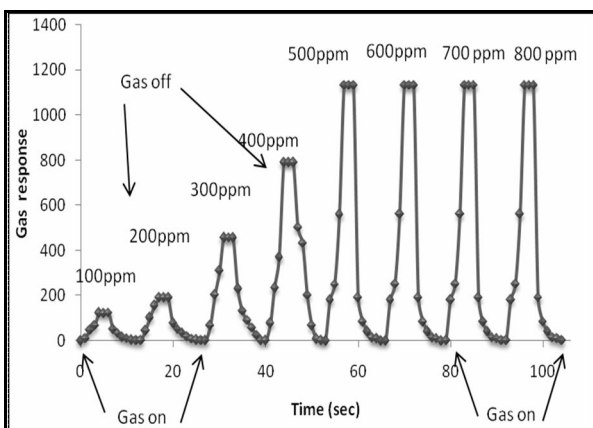### 5.3. Response and recovery of the sensor with concentration of gas in ppm

Figure 9: Response and recovery of the sensor for most sensitive sample (S4).

The response and recovery of the WO_3-V_2O_5 nanocomposites thin film (S4) sensor on exposure of 500 ppm of SO_2 at 350 °C are represented in Fig. 9. The response is quick (4 s) and recovery is fast (8 s). The high oxidizing ability of adsorbed oxygen species on the surface nanoparticles and high volatility of desorbed by-products explain the quick response to H_2S and fast recovery [21].
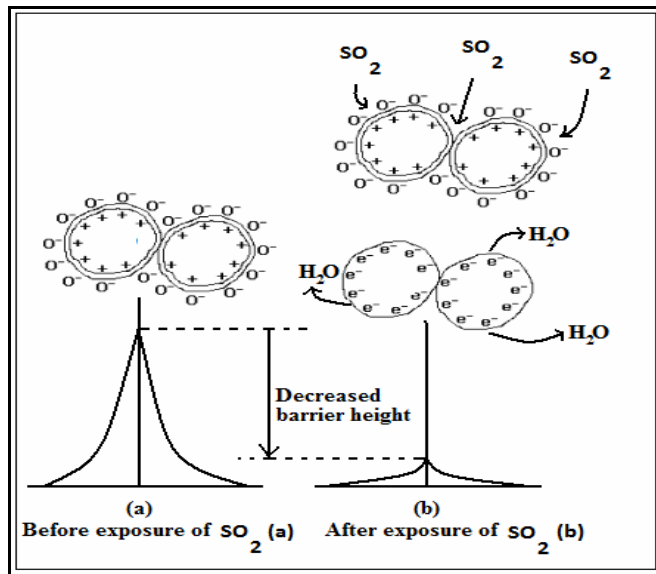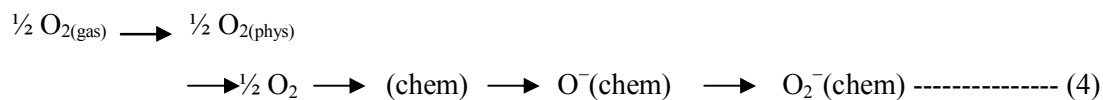
6. Discussion

6.1. Gas sensing mechanism

Figure 10:.Shows gas sensing mechanism (before exposure and after exposure of SO$_2$ gas) for WO$_3$-V$_2$O$_5$ nanocomposites thin film

The gas response of any metal oxide semiconductor to a particular gas increases with the decrease in the size of nanocrystallites [27] due to an increase in surface to volume ratio. Grain sizes and microstructures of the sensor affect the gas sensing performance of the sensor. It was found that, if the grain size of the sensor material is sufficiently small, the area of active surface sites is larger, and the sensitivity and selectivity for a particular gas enhances largely [28].

According to the present understanding on the response of semiconductor gas sensors, the change in the electrical resistance is closely related to the chemical properties of the surface oxygen. In the aerial atmosphere where the partial pressure of oxygen is taken as constant, oxygen is adsorbed on WO$_3$-V$_2$O$_5$ surfaces in different forms depending on the temperature, usually from physisorption to chemisorption (including entering the crystal lattice), that is, from molecular form to dissociative form as temperature increases.

$$\frac{1}{2} O_{2(gas)} \longrightarrow \frac{1}{2} O_{2(phys)}$$

$$\longrightarrow \frac{1}{2} O_2 \longrightarrow (chem) \longrightarrow O^-(chem) \longrightarrow O_2^-(chem) \text{ --------------- (4)}$$

These oxygen adsorbates (O$_{2-}$, O$^-$ and O^{2-}) on the surface of WO$_3$-V$_2$O$_5$ can induce an electron-depleted surface region, resulting in the increase in surface potential barrier and electrical resistance, as depicted schematically in Figure 10 (a). Upon exposures to reducing gases like SO$_2$, the surface oxygen is consumed due to the chemical reaction, donating a few electrons back and thus leading to the decrease in potential barrier (Fig. 10 (b)) and then also in electrical resistance, where the concentration of surface oxygen shifts from the steady-state value in air to a new steady value, depending monotonically on the concentration of the gas. The chemical adsorption of oxygen and its reaction with reducing gases underlie the sensing mechanism of WO$_3$-V$_2$O$_5$ nanocomposites toward SO$_2$ gases.

In case of semiconductors metal oxide, their surface metal ions capture an extra electron (acts as an acceptor) and the surface oxygen ions give up an electron (act as donor). The donor levels are completely ionized if they are near the conduction band; however, if the donor levels are little below the conduction band, the donor levels are not completely ionized at room temperature. Donor levels get ionized above room temperature.

7. Conclusions

WO$_3$, V$_2$O$_5$, and WO$_3$-V$_2$O$_5$ nanocomposites thin films were prepared by simple spray pyrolysis technique. The structural and morphological properties confirm that the as-prepared WO$_3$, V$_2$O$_5$, and WO$_3$-V$_2$O$_5$ nanocomposites thin films are nanostructured in nature. The elemental analysis conferred that as prepared thin films were nonstoichiometric in nature. The WO$_3$-V$_2$O$_5$thin film of (Sample S4) was most sensitive to SO$_2$ gas and exhibits the response of S = 1130 to the gas concentration as 500 ppm at the temperature of 350 ^{o}C. The sensor has good selectivity to SO$_2$ against LPG, CO$_2$, H$_2$, NH$_3$, C$_2$H$_5$OH, acetone, Cl$_2$.and H$_2$S.The WO$_3$-V$_2$O$_5$nanocomposites thin films exhibit rapid response–recovery which is one of the main features of this sensor.

Acknowledgements

Reference

1. L. Ottaviano, L. Lozzi, M. Passacantando, and S. Santucci, "On the spatially resolved electronic structure of polycrystalline WO$_3$ films investigated with scanning tunneling spectroscopy," Surface Science, 475, pp. 73-82, 2001.
2. L. J. LeGore, R. J. Lad, S. C. Moulzolf, J. F. Vetelino, B. G. Frederick, and E. A. Kenik, "Defects and morphology of tungsten trioxide thin films," Thin solid films, 406, pp. 79- 86, 2002.
3. N. Soultanidis, W. Zhou, Ch.J. Kiely, and M.S. Wong, "Solvothermal Synthesis of ultrasmall tungsten oxide nanoparticles", Langmuir, 28, pp. 17771-17777,2012.
4. C. G. Granqvist, "Electrocrhomic tungsten oxide films: review of progress 1993-1998," Solar Energy Materials & Solar Cells, 60, pp. 201-262, 1999.
5. A. Di Paola, L. Palmisano, A. M. Venezia, and V. Augugliano, "Coupled semiconductor systems for photocatalysis. Preparation and characterization of polycrystalline mixed WO3/WS2 powders," J. Phys. Chem. B, 103, pp. 8236-8244, 1999.
6. A. Löfbeg, A. Frennet, G. Leclercq, L. Leclercq, and J. M. Giraudon, "Mechanism of WO$_3$ reduction and carburization in CH$_4$/H$_2$ mixtures leading to bulk tungsten carbide powder catalysts," Journal of Catalysis, 189, pp. 170-183, 2000.
7. G. Eranna, B. C. Joshi, D. P. Runthala, and R. P. Gupta, "Oxide Materials for development of integrated gas sensors - a comprehensive review," Critical reviews in Solid State and Materials Sciences, 29, pp. 111-188, 2004.
8. P. J. Shaver, "Activated tungsten oxide gas detector," Appl. Phys. Lett., 11, pp. 255-256, 1967.
9. U. Schlecht, I. Besnard, A. Yasuda, T. Vossmeyer, M. Burghard, in: H. Kuzmany, J. Fink, M. Mehring, S. Roth (Eds.), Molecular Nanostructures: XVII Int'l. Winterschool/Euroconference on Electronic Properties of Novel Materials, vol. CP685, American Institute of Physics, Melville, NY, 2003, p. 491.
10. J. Muster, G.T. Kim, V. Krstic, J.G. Park, Y.W. Park, S. Roth, M. Burghard, "Electrical transport through individual vanadium pentoxide nanowires", Adv. Mater. 12, pp. 420–424, 2000.
11. G.T. Kim, J. Muster, V. Krstic, J.G. Park, Y.W. Park, S. Roth, M. Burghard, "Fieldeffect transistor made of individual V$_2$O$_5$ nanofibers", Appl. Phys. Lett. 76, pp.1875–1877, 2000.
12. P. Mitra and A.K. Mukhopadhyay, "ZnO thin film as methane sensor", Bulletin of the. Polish Academy of Sciences: Technical Sciences, 55, pp. 281–285, 2007.
13. T. Jinkawa, G. Sakai, J. Tamaki, N. Miura, N. Yamazoe, "Relationship between ethanol gas sensitivity and surface catalytic property of tin oxide sensors modified with acidic or basic oxides", J. Mol. Catal. A Chem., 155, pp. 193–200, 2000.
14. P.R. Makgwane, S.S. Ray, "Efficient room temperature oxidation of cyclohexane over highly active hetero-mixed WO$_3$/V$_2$O$_5$ oxide catalyst", Catalysis Communications 54, pp.118–123, 2014.

15.   [15] N. Yamazoe, Gas Sensors, Principles, "Operation and development", Sens.Actuators B, 108, 2 2005.

16.   C.N. Xu, J. Tamaki, N. Miura, N. Yamazoe, "Grain size effects on gas sensitivity of porous SnO₂-based elements", Sens. Actuators B, 3, pp.147–155. 1991.

17.   E. Comini, G. Faglia, G. Sberveglieri, Z. Pan, Z.L.Wang, "Stable and highly sensitive gas sensors based on semiconducting oxide nanobelts"Appl. Phys. Lett., 81, pp.1869-1871, 2002.

18.   Y. Wang, X. Jiang, Y. Xia, "A solution-phase", J. Am. Chem. Soc., 125, pp,16176 -16177 2003.

19.   S. Chakraborty, A. Sen, H.S. Maiti, "Selective detection of methane and butane by temperature modulation in iron doped tin oxide sensors", Sens. Actuators B, 115, pp. 610–613, 2006.

20.   Y. Shimizu, E.D. Bartolomeo, E. Traversa, G. Gusmano, T. Hyodo, K. Wada, M. Egashira, "Effect of surface modification on NO₂ sensing properties of SnO₂ varistor-type sensors", Sensors and Actuators B, 60, pp.118–124, 1999.

21.   R. H. Bari, S. B. Patil, A.R. Bari, G. E. Patil, J. Aambekar, "Spray pyrolysed nanostructured ZnO thin film sensors for ethanol gas" Sensors & Transducers Journal, 140, pp.124-132, 2012.

22.   JCPDS card no. 01-075-2187

23.   JCPDS card no.00-054-0513.

24.   S. M. Patil, P. H. Pawa, "Nanocrystalline hexagonal shaped CdS thin films for photoconducting application", 36, pp 153-167, 2014.

25.   G. E. Patil, D. D. Kajale, D. N. Chavan, N. K. Pawar, P. T. Ahire, S. D. Shinde, V. B. Gaikwad, "Synthesis, characterization and gas sensing performance of SnO2 thin films prepared by spray pyrolysis", Bull. Mater. Sci., 34, 1-9, 2011

26.   P.P. Sahay,"Zinc oxide thin film gas sensor for detection of acetone", J. Mater. Sci.40, 4383-4388, 2005.

27.   L.A. Patil, A.R. Bari, M.D. Shinde, Vinita Deo and M.P. Kaushik, "Detection of dimethyl methyl phosphonate – a simulant of sarin: the highly toxic chemical warfare –using platinum activated nanocrystalline ZnO thick films", Sensors and Actuators B: Chemical, 161, pp.372–380, 2012.

28.   L.A. Patil, A.R. Bari, M.D. Shinde, Vinita Deo, "Ultrasonically prepared nanocrystalline ZnO thin films for highly sensitive LPG sensing" Sensors and Actuators B: Chemical, 149, pp.79-86, 2010.

✷✷✷✷✷